

The APM Galaxy Survey. IV: Redshifts of Rich Clusters of Galaxies

G. B. Dalton, G. Efstathiou, S. J. Maddox & W. J. Sutherland*

Department of Physics, University of Oxford, Keble Road, Oxford, OX1 3RH. UK.

16 November 1993

ABSTRACT

We present redshifts for a sample of 229 clusters selected from the APM Galaxy Survey, 189 of which are new redshift determinations. Non-cluster galaxy redshifts have been rejected from this sample using a likelihood ratio test based on the projected and apparent magnitude distributions of the cluster fields. We test this technique using cluster fields in which redshifts have been measured for more than 10 galaxies. Our redshift sample is nearly complete and has been used in previous papers to study the three dimensional distribution of rich clusters of galaxies. 157 of the clusters in our sample are listed in the Abell catalogue or supplement, and the remainder are new cluster identifications.

Key words: Galaxy Clusters: Catalogues, Galaxies: Redshifts, Cosmology: Large-Scale Structure.

1 INTRODUCTION

Clusters of galaxies can provide much information on the large-scale distribution of matter in the universe. The cluster catalogues of Abell (1958), Zwicky *et al.* (1968) and Abell, Corwin & Olowin (1989) were constructed by visual inspection of sky survey plates, and have been used widely to investigate cluster properties, galaxy evolution, and the large-scale structure of the universe.

Studies of the three-dimensional distribution of clusters in the Abell catalogues have shown that it is anisotropic, with an excess number of cluster pairs found with small angular separations but large radial separations (Sutherland 1988; Sutherland & Efstathiou 1991; Efstathiou *et al.* 1992). This effect may be an artefact either of the process of selecting galaxy clusters from inhomogeneous plate material, of the enhancement of a cluster due to the overlap of adjacent cluster halos (Dekel *et al.* 1989), of the process of selecting clusters by eye over long periods, or of patchy Galactic extinction or contamination by ‘clusters’ which are simply projected associations along the line of sight (Peacock & West 1992). This effect produces more power on large scales than is predicted by models where structure forms by purely gravitational mechanisms, given the observed amplitude of the galaxy autocorrelation function (Maddox, Efstathiou & Sutherland 1993)

We have constructed cluster catalogues from the APM Galaxy Survey (Maddox *et al.* (1990a,b)) with the aim of im-

proving on Abell’s catalogues and resolving the issue of the large-scale clustering of clusters. In this paper we list new measurements of redshifts for galaxies in 189 clusters, and a catalogue of 229 cluster redshifts. This catalogue encompasses the cluster sample used for the determination of the correlation amplitude for the APM clusters (Dalton *et al.* 1992; Efstathiou *et al.* 1992). In §2 we give a brief description of the cluster selection algorithm. In §3 we describe the maximum likelihood estimator for the cluster distance which we use to test our redshift observations for the presence of foreground galaxies. The observations are discussed in §5 and we summarise our observations and discuss further extension of the survey in §6.

2 THE CLUSTER CATALOGUE

The APM Galaxy Survey (Maddox *et al.* (1990a,b)) is based on scans of 185 UK Schmidt J plates with the SERC Automatic Plate Measuring (APM) machine and lists accurate positions and magnitudes for over 2 million galaxies brighter than a magnitude limit of $b_J = 20.5$, with completeness $\sim 90\text{--}95\%$, stellar contamination $\sim 5\%$ and negligible dependence of the galaxy surface density on declination or galactic latitude. The survey covers a solid angle of 4300 square degrees.

Clusters of galaxies were selected from the APM Survey using a two-stage process (a detailed description will be given in paper V in this series). The first stage involves locating dense spots in the galaxy surface density above a magnitude limit $b_J = 20.5$ by applying a percolation algorithm linking together galaxies with angular separations less

* Current Address: Center for Particle Astrophysics, University of California, Berkeley, Ca 94720, USA.

than 0.7 times the mean separation. This algorithm was applied separately to each photometrically matched Schmidt plate, and groups containing ≥ 20 galaxies were chosen as candidate cluster centers.

In the second stage, an iterative procedure was applied to define a characteristic magnitude m_X and richness \mathcal{R} for each cluster as described by Dalton *et al.* (1992). The cluster selection algorithm is objective, and improves on Abell's selection in several ways. Our smaller counting radius (half the Abell radius) and the weighting scheme improve the contrast above background and reduces the overlap area of neighbouring cluster halos and the associated ambiguity of assigning galaxies to clusters in supercluster regions.. Using our characteristic magnitude, m_X , instead of Abell's m_{10} means that the distance estimate should be nearly independent of cluster richness. The high photometric accuracy of the APM Survey should yield m_X estimates and richnesses that are uniform over the entire area of the survey.

3 CLUSTER DISTANCES USING MAXIMUM LIKELIHOOD

3.1 Cluster Model

In order to arrive at an estimator for the cluster distance we first adopt a model for the galaxy distribution within the cluster field. We adopt a Schechter function for the galaxy luminosity function, with parameters determined by Loveday *et al.* (1992):

$$\phi(L)dL = \phi_*(L/L_*)^\alpha \exp(-L/L_*)dL/L_*, \quad (1)$$

$$B_{J*} = -19.6; \quad \phi_* = 1.2 \times 10^{-2} h^3 \text{Mpc}^{-3}; \quad \alpha = -1.08.$$

We will discuss the choice of these parameters in §5. The mean galaxy density at redshift z is then given by

$$\begin{aligned} \bar{n} &= \phi_* \int_{x_{lim}(z)}^{\infty} x^\alpha \exp(-x) dx, \\ &= \phi_* \Gamma(\alpha + 1, x_{lim}(z)), \\ x_{lim}(z) &= L_{min}(z, m_{lim})/L_*, \end{aligned} \quad (2)$$

where $L_{min}(z, m)$ is the minimum luminosity visible at a redshift z , given an apparent magnitude limit of m .

We assume that the luminosity of a cluster galaxy is independent of position within the cluster, and so our cluster model may be expressed in terms of separate functions of apparent magnitude and radial position. As an estimate of a mean cluster radial profile we take the form of the cluster-galaxy cross-correlation given by Lilje & Efstathiou (1988)

$$\xi_{cg}(r) = (r/r_0)^{-\epsilon}; \quad \epsilon = 2.2, r_0 = 8.8 h^{-1} \text{Mpc}, \quad (3)$$

where, for the purposes of the model, we will assume that $\xi_{cg} \equiv 0$ beyond a limiting radius r_T .

The surface density of galaxies around the cluster centre may be expressed as

$$\begin{aligned} \mu(\sigma) &= 2 \int_0^\infty n(r) dy \\ r^2 &= \sigma^2 + y^2, \end{aligned} \quad (4)$$

where σ and y are the components of the radial vector on the sky and along the line of sight, respectively.

Inserting (3) into (4) and assuming $\xi_{cg} \gg 1$ gives

$$\mu(\sigma) = \frac{\bar{n} r_0^\epsilon}{\sigma^{\epsilon-1}} \int_0^{r_T/\sigma^2-1} \frac{t^{-1/2} dt}{(1+t)^{\epsilon/2}}. \quad (5)$$

In all cases of interest we have $\sigma \ll r_T$, and so

$$\mu(\sigma) \approx \frac{\bar{n} r_0^\epsilon}{\sigma^{\epsilon-1}} \int_0^\infty \frac{t^{-1/2} dt}{(1+t)^{\epsilon/2}}. \quad (6)$$

The number of galaxies associated with the cluster is then

$$N_c(\sigma) = 2\pi^2 r_0^\epsilon \phi_* \Gamma(\alpha + 1, x_{lim}(z)) \frac{\Gamma((\epsilon-1)/2)}{\Gamma(\epsilon/2)} \frac{\sigma^{3-\epsilon}}{(3-\epsilon)}. \quad (7)$$

Note that in this equation we have assumed that the galaxy luminosity function is the same for galaxies in clusters and in the field. We shall return to this question later.

3.2 The Maximum Likelihood Estimator

From equation 7 the total number of galaxies belonging to a cluster at redshift z predicted to lie within a projected radius θ to a limiting magnitude m is

$$N_c(\theta, m) = A(z) \Gamma(\alpha + 1, x_{min}(z, m)) \theta^{3-\epsilon}, \quad (8)$$

and from the field,

$$N_f(\theta, m) = B(z) \theta^2. \quad (9)$$

Here we have defined

$$A(z) = \frac{2\pi^2 \phi_* r_0^\epsilon}{3-\epsilon} \frac{\Gamma((\epsilon-1)/2)}{\Gamma(\epsilon/2)} (d_A(z))^{3-\epsilon}, \quad (10a)$$

$$d_A(z) = y(z)/(1+z), \quad (10b)$$

$$B(z) = \pi \phi_* \int_0^\infty \int_{x_{min}(z, m)}^\infty x^\alpha e^{-x} dx y^2 dy, \quad (10c)$$

$$x_{min}(z, m) = 10^{0.4(m_*(z) - m)}, \quad (10d)$$

$$m_*(z) = M_* + 25 + 5 \log(d_l(z)) + K_z z, \quad (10e)$$

$$d_l(z) = (1+z)y(z), \quad (10f)$$

where we adopt a K-correction term of $K_z = 3.0$. Differentiating equations 8 and 9 gives

$$\frac{dN_c(\theta, m)}{d\theta dm} = 0.4 \ln(10) A(z) (3-\epsilon) \theta^{(2-\epsilon)} [x_m^\alpha \exp(-x_m)] \quad (11)$$

$$\frac{dN_f(\theta, m)}{d\theta dm} = 0.8 \ln(10) \pi \phi_* \theta \int_0^\infty x_m^{\alpha+1} \exp(-x_m) y^2 dy, \quad (12)$$

so that for each galaxy found within a circle of radius θ_f we can define the quantity

$$p_i = N_g \frac{dN_c(\theta_i, m_i) + dN_f(\theta_i, m_i)}{N_c(\theta_f, m_{lim}) + N_f(\theta_f, m_{lim})}, \quad (13)$$

where N_g is the total number of galaxies found within θ_f , and hence we may define the likelihood of the field representing a cluster at redshift z by

$$\mathcal{L} = \prod_i p_i, \quad (14)$$

and obtain an estimate of the cluster redshift by maximising $\mathcal{L}(z)$.

Equation (13) assumes that the field galaxy distribution is unclustered, and that all clusters have the same richness. To modify the first of these assumptions we obtain the field normalisation, α , by determining the ratio of the local galaxy background surface density around the cluster to that predicted for a uniform distribution with our input luminosity function. The normalisation of the cluster model is then fixed by the total number of galaxies in the field to be

$$\beta = \frac{N_g - \alpha N_f(\theta_f, m_{lim})}{N_c(\theta_f, m_{lim})}, \quad (15)$$

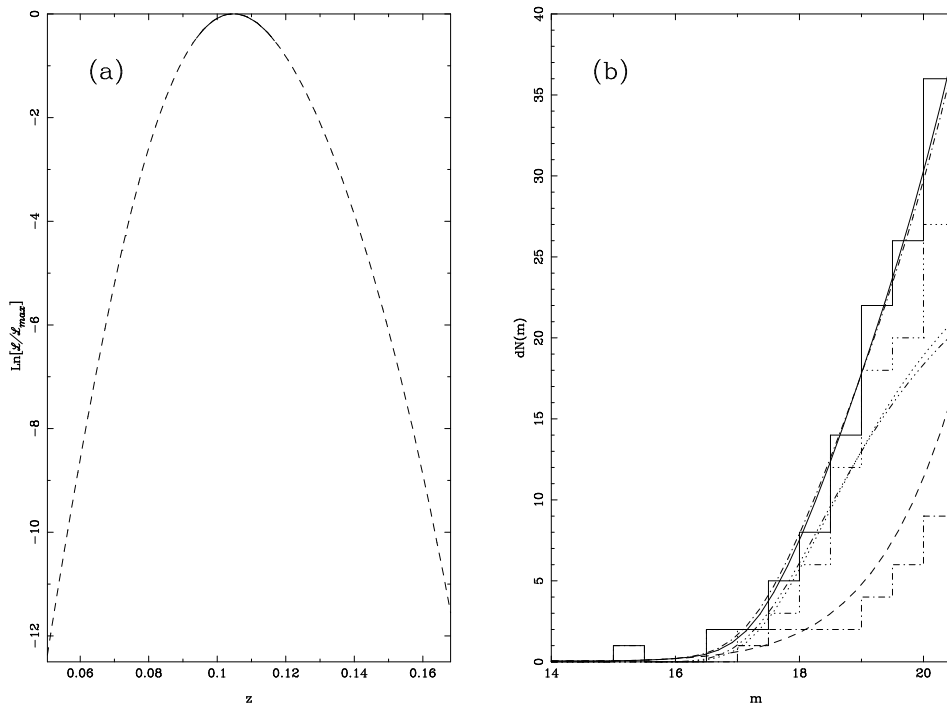


Figure 1. a) The likelihood function for a model cluster generated with $z = 0.1$. The solid part of the curve represents a $1\text{-}\sigma$ interval as described in the text. The likelihood function is maximised for $z = 0.1042$. b) The apparent magnitude distribution of the field of the cluster (solid histogram), made up of cluster (dot-dot-dashed) and field (dot-dashed) components. The solid line shows the apparent magnitude distribution for the maximum likelihood redshift, with cluster and field components shown (dotted and dashed lines, respectively). The dot-dashed and dot-dot-dot-dashed lines show the model predictions for the total apparent magnitude distribution and cluster component given $z = 0.1$, given the adopted background.

which may be used as an alternative estimate of the cluster richness. We can now rewrite (13) as

$$p_i = N_g \frac{\beta dN_c(\theta_i, m_i) + \alpha dN_f(\theta_i, m_i)}{\beta N_c(\theta_f, m_{lim}) + \alpha N_f(\theta_f, m_{lim})}. \quad (16)$$

3.3 Some Examples

We generated a set of model clusters using the model described above to give an estimate of the accuracy of the redshift estimator, and to provide comparison data for real cluster fields. The likelihood function for one model cluster is shown in Fig.1a. The estimated redshift agrees well with the true redshift for the cluster. In Fig.1b we show the apparent magnitude distribution of the cluster and field components compared to those predicted for the redshift of maximum likelihood. Since, in the limit of large numbers, the quantity $-2 \ln \mathcal{L}/\mathcal{L}_{max}$ is expected to approximate χ^2 distributed with 1 degree of freedom we obtain a $1\text{-}\sigma$ confidence interval by computing the range of redshifts for which $\ln \mathcal{L}/\mathcal{L}_{max} \geq -0.49$, this interval is represented by the solid part of the curve in Fig.1a. We repeated the analysis for a set of 228 model clusters with redshifts in the range $0.002 \leq z \leq 0.2$, distributed as $z^2 dz$. The scatter over the whole range of redshifts was $\sigma_z = 0.018$, or 0.009 if we restricted observations to clusters in the range $z \leq 0.12$. There was no systematic trend with redshift.

As examples of how this technique can be applied to real data, we have analysed two Abell clusters, taken more-

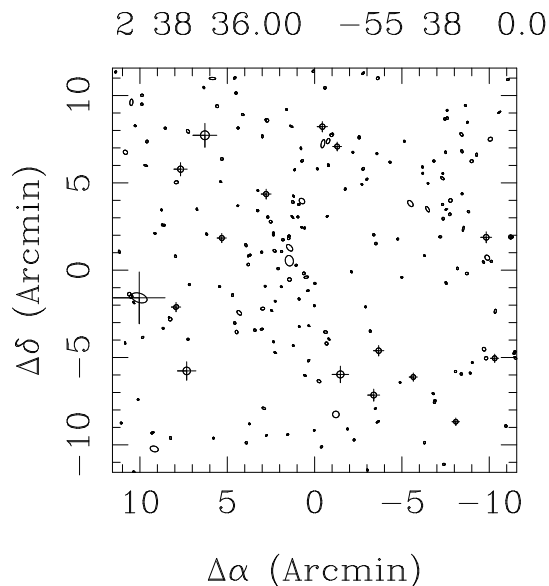


Figure 2. The field of view of the cluster A3040 as seen in the APM Survey data. The limiting magnitude of the plot is $b_J = 20.65$. The documented redshift is for the large galaxy in the centre of the field.

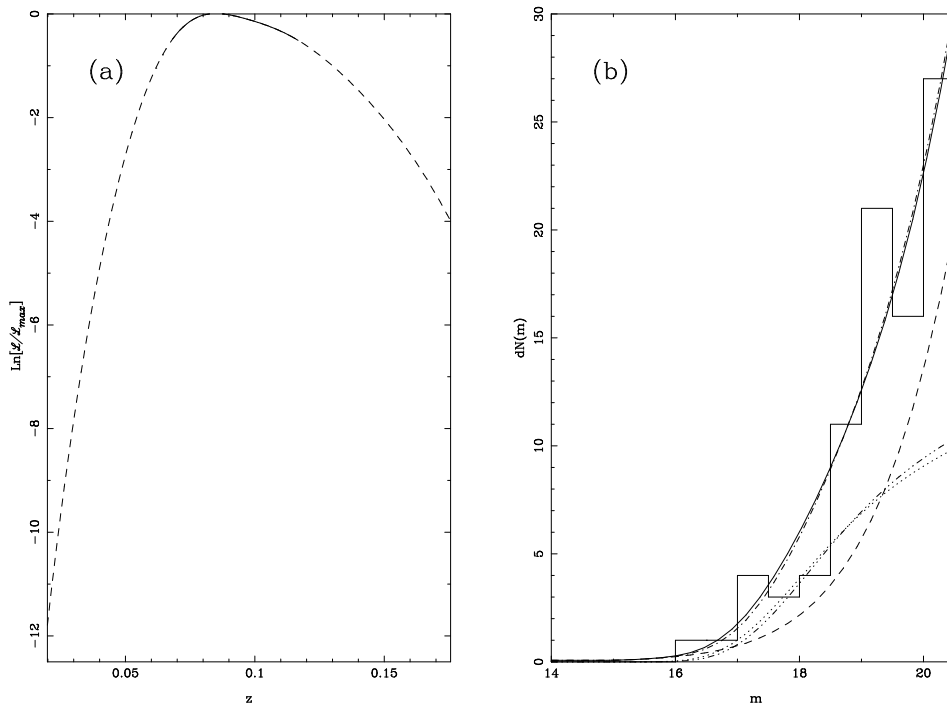


Figure 3. a) The likelihood function for A3040. The likelihood function is maximised for $z = 0.0878$. b) The apparent magnitude distribution for A3040. Components corresponding to the model predictions for the field and both the maximum likelihood and listed redshifts are shown as in fig. 1b.

or-less at random from the literature. The field of the cluster A3040, which has a redshift of $z = 0.093$ (West & Fransden 1981) is shown in Fig.2. The likelihood function and apparent magnitude distribution for this cluster are shown in Fig.3. Comparing Fig.1 with Fig.3 shows that the likelihood function is somewhat less strongly peaked for real data, which in turn should imply a larger spread of errors in the redshift estimates when the estimator is applied to a number of real clusters.

As another example we consider the cluster A2860, listed redshift $z = 0.0268$ (Abell, Corwin & Olowin 1989). The likelihood function (Fig.4a) for this cluster peaks beyond $z = 0.1$, and agrees well with our multi-fibre observations as described in the next section. Fig.5 shows the field of this cluster. Of the 12 galaxies for which good spectra were obtained, 10 have redshifts $z \sim 0.1$. The model predictions for a cluster at $z = 0.0268$ are shown in Fig.4b. The likelihood ratio test gives zero probability for the field to represent a cluster at this redshift. Using our observed redshift as input gives a maximum likelihood redshift estimate of $z_{\mathcal{L}} = 0.0975$, for which our observed $z = 0.106$ gives a likelihood ratio of 0.94 corresponding to a 71% probability for the field to contain a cluster this redshift.

3.4 Application

We apply the maximum likelihood estimator to each cluster interactively. The field of each cluster is initially set to correspond to $0.75 h^{-1} \text{Mpc}$ at the redshift to be tested. The value of the background normalisation is defined by the ratio of the observed counts in annuli out to 1.5° to the galaxy

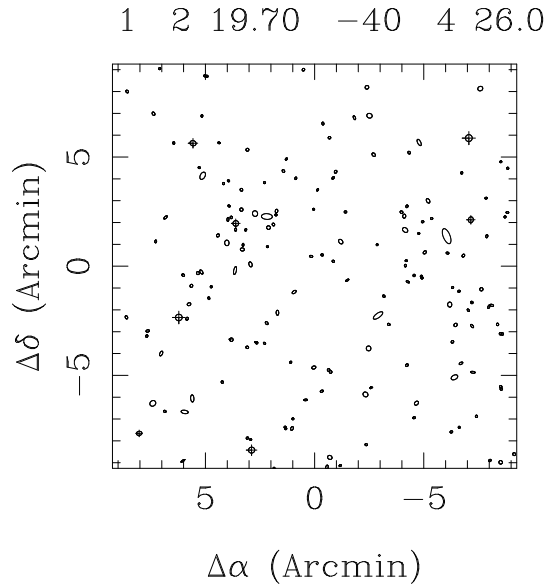


Figure 5. The field of view of the cluster A2860 as seen in the APM Survey data. The limiting magnitude of the plot is $b_J = 20.6$. 10 of the brighter galaxies in this field have redshifts $z \sim 0.106$.

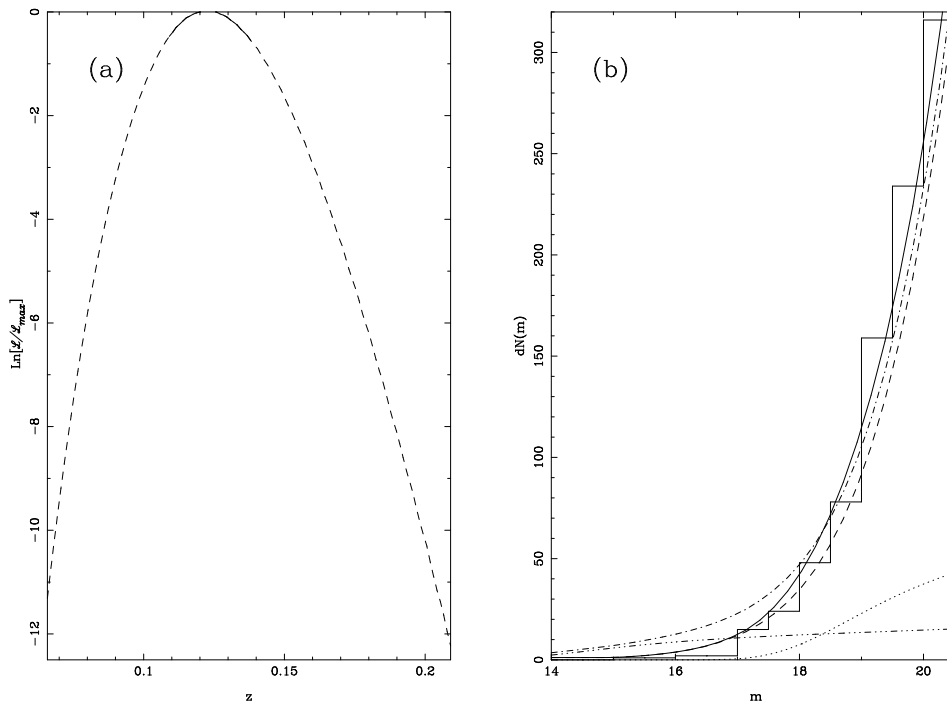


Figure 4. a) The likelihood function for A2860 generated using the galaxy distribution within a circle of projected radius $r_C = 0.75 h^{-1} \text{Mpc}$ at the listed redshift of $z = 0.0268$. b) The apparent magnitude distribution for A2860 showing the model predictions for both the maximum likelihood and input redshifts.

number counts inferred from our model for the field component. If the redshift of maximum likelihood suggests that the galaxy in question is foreground to the cluster then we repeat the analysis using the maximum likelihood redshift to obtain a new projected radius for the field.

In some cases the likelihood function is found to have more than one peak due to the presence of a single very bright galaxy. We therefore test each cluster for contamination of the likelihood function by bright galaxies by successively removing the brightest galaxies from the field to obtain a stable redshift estimate.

4 EXISTING REDSHIFT DATA

From our cluster catalogue, we selected a target sample of 240 clusters with $\mathcal{R} \geq 20$ and photometrically derived redshifts $z_X \leq 0.1$. Our aim was to determine redshifts for all of these clusters. We began by cross-correlating all 122 clusters from Andernach's compilation which were found within the APM Survey region. We applied the maximum likelihood analysis of §3 to each of these clusters to give an estimate of the cluster redshift in each case, and the likelihood ratio test was used to reject documented redshifts as described above. Where positional information was available from the literature we also inspected the galaxies for which redshifts had been obtained, and rejected all those which appeared to be foreground objects such as bright spirals or galaxies far from the cluster centres.

We cross-referenced the resulting 'decontaminated' list with our target catalogue and obtained 36 redshifts. These are listed in Table 1. We stress that these are not the only

Abell clusters with reliable documented redshifts in the APM Survey region, but simply those which are matched to clusters in our target sample. Five clusters in this table have no identification in our catalogue, but are retained as they represent nearby systems which are at low contrast on the sky, and so are missed by the initial stage of the cluster selection process. The relationship between redshift and m_X for the matched clusters is shown in Fig. 6. The best fit relation is

$$\log z = -3.523 + 0.133m_X$$

with a scatter of 0.08 in $\log z$.

5 THE REDSHIFT SURVEY

Our initial observing strategy was to obtain redshifts using a multiplexed setup to observe at least 10 galaxies per cluster. We observed 23 APM clusters in October 1989 using the AUTOFIB system and Image Photon Counting System (IPCS) at the Anglo-Australian Telescope (AAT) with wavelength coverage of 3670\AA - 5680\AA and $2\text{\AA}/\text{pixel}$, giving redshifts for $\gtrsim 20$ galaxies per cluster in 3 nights of observing. Redshifts were determined from a sample of stellar templates using the cross-correlation technique of Tonry & Davis (1979), with a lower threshold for acceptance of the redshift set at $r = 2.5$, where r is the signal to noise ratio of the peak in the cross-correlation function as defined by Tonry & Davis. In a few cases galaxy redshifts were determined from emission line features, but these are rare given that we restricted our observations to early-type galaxies. The AUTOFIB clusters are listed in table ???. Entries in

Table 1. Clusters for which redshifts were found in Anderson's compilation after rejection of probable redshift mis-identifications. Those clusters with no entries in columns 3 and 4 are nearby systems which could be missed in the percolation stage of our cluster selection procedure.

(1) $\alpha(1950)$	(2) $\delta(1950)$	(3) m_X	(4) \mathcal{R}	(5) z	(6) Abell
00 03 43.51	-34 59 05.27	19.083	69.943	0.116	A2721
00 18 01.94	-49 33 47.53	17.608	30.170	0.064	A2764
00 18 04.13	-25 58 36.48	19.396	72.301	0.131	A0022
00 23 00.67	-33 19 18.12	16.701	30.030	0.050	S0041
00 26 07.54	-23 53 19.32	19.227	45.402	0.109	A0042
01 00 19.56	-22 09 07.92	17.988	38.168	0.060	A0133
01 07 40.08	-46 10 28.56	15.983	31.139	0.023	A2877
02 49 15.29	-25 07 54.84	18.654	74.823	0.116	A0389
03 06 03.12	-23 52 49.44	—	—	0.041	A0419
03 14 51.84	-51 05 56.40	17.940	31.065	0.075	A3110
03 16 09.82	-44 25 16.68	18.258	49.031	0.072	A3112
03 17 54.00	-54 02 60.00	—	—	0.055	S0339
03 25 59.02	-53 53 06.72	17.017	39.791	0.059	A3125
03 27 23.50	-55 52 41.88	18.766	91.874	0.086	A3126
03 29 07.94	-52 43 04.08	17.264	59.761	0.059	A3128
03 39 05.30	-55 13 12.00	—	—	0.043	S0377
03 41 42.29	-53 47 57.84	18.082	62.224	0.058	A3158
03 43 38.88	-24 25 58.44	19.110	48.669	0.105	A0458
04 30 31.78	-61 31 51.96	18.120	47.493	0.059	A3266
04 36 36.29	-22 14 26.16	17.560	47.456	0.067	A0500
04 46 10.44	-20 33 14.40	17.819	45.751	0.073	A0514
04 59 03.99	-22 53 01.32	—	—	0.047	A0533
20 35 36.36	-61 24 36.36	16.742	43.854	0.071	A3703
20 38 44.14	-35 25 40.81	18.300	62.379	0.090	A3705
20 48 07.92	-52 56 04.92	15.741	44.932	0.047	S0906
21 31 03.56	-53 51 02.52	17.591	32.325	0.078	A3785
21 49 31.83	-19 48 40.32	19.327	69.692	0.094	A2384
21 58 17.90	-60 11 05.63	18.470	40.567	0.099	A3827
22 17 02.14	-55 28 18.84	—	—	0.040	A3869
22 21 29.66	-64 30 37.44	18.967	39.439	0.094	S1022
22 30 05.18	-55 03 49.33	18.779	41.799	0.075	A3886
22 59 33.70	-22 17 02.76	19.338	50.752	0.136	A2521
23 02 54.94	-21 38 42.36	18.295	35.898	0.095	A2528
23 05 55.22	-20 09 28.44	18.780	51.898	0.083	A2538
23 09 36.52	-21 50 16.80	18.809	61.707	0.086	A2556
23 56 20.59	-60 55 55.20	19.318	47.358	0.096	A4067

this table which have no entries for \mathcal{R} or m_X were included in the original selection for this run, and were retained in our final sample for the same reasons as the nearby Abell clusters from table 1.

The data from these observations, together with additional multi-object data from Colless & Hewett (1987) and Teague, Carter & Gray (1990) suggested that restricting observations to the brightest pair of early-type galaxies within our cluster defining radius would give the correct cluster redshifts with only a small number of contaminants. The data are shown in figure 7. Applying the likelihood ratio test of §3 to these clusters rejected only those redshifts which are shown as open symbols. This shows that the likelihood ratio test succeeds in rejecting all foreground galaxies. The residual scatter of the solid points in figure 7 is 512km s^{-1} .

We therefore adopted as optimal the strategy of observing only one pair of galaxies for each remaining cluster using a single slit oriented to observe both galaxies simultaneously.

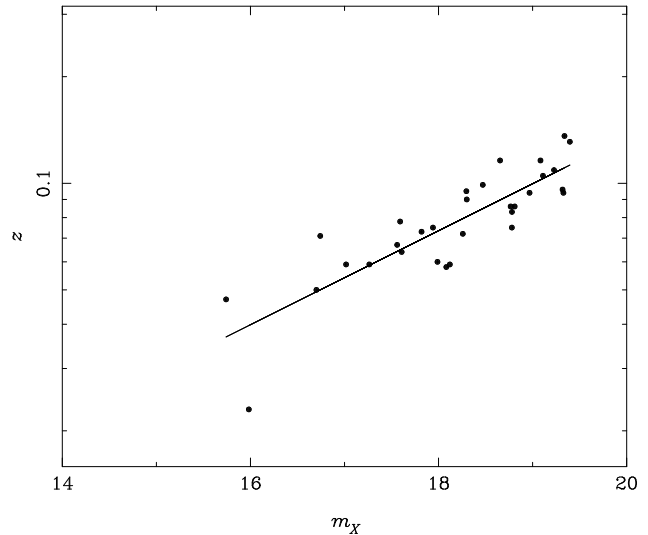


Figure 6. The relationship between redshift and m_X for the sample of clusters with documented redshifts.

Table 2. Clusters observed using AUTOFIB. Column (6) gives the number of galaxies for which redshifts were obtained in each field. Clusters with no entries in columns (3) or (4) were included in the original selection for the AUTOFIB observations and are included in our final list as nearby systems (see text).

(1) $\alpha(1950)$	(2) $\delta(1950)$	(3) m_X	(4) \mathcal{R}	(5) z	(6) N_z	(7) Abell
00 35 04.8	-28 47 53	18.918	34.944	0.113	21	A2798
00 46 53.9	-29 47 54	19.011	51.255	0.108	18	S0084
01 02 19.7	-40 04 26	18.096	34.959	0.106	12	A2860
01 12 00.9	-32 06 26	15.714	21.800	0.020	14	S0141
01 29 24.6	-51 37 9	16.260	22.095	0.055	19	S0162
01 39 44.7	-42 23 32	17.587	30.208	0.076	15	S0180
02 28 32.8	-33 19 32	18.389	37.181	0.076	21	A3027
03 09 42.7	-53 13 26	—	—	0.053	18	
03 35 37.1	-55 10 46	16.697	25.683	0.045	16	A3144
04 52 31.0	-18 22 36	—	—	0.030	16	
20 57 24.6	-38 47 54	—	—	0.046	17	A3733
20 58 43.6	-28 18 23	16.533	26.885	0.038	22	
20 59 36.7	-41 34 46	16.527	26.950	0.082	16	A3739
21 08 08.7	-23 20 32	15.867	29.690	0.033	15	
21 46 34.5	-55 35 29	16.482	25.542	0.036	17	A3816
21 50 18.2	-55 50 49	—	—	0.036	17	A3816
21 59 39.3	-22 50 22	17.501	53.990	0.070	15	S0987
22 15 39.0	-39 08 17	19.315	44.986	0.126	2	A3856
22 24 19.2	-30 49 1	17.140	37.057	0.057	10	A3880
22 34 18.7	-38 16 49	19.337	37.279	0.105	10	S1045
23 28 01.3	-35 20 21	16.638	21.957	0.050	17	A4013
23 44 19.7	-28 27 16	16.173	22.113	0.029	30	A4038
23 53 35.5	-34 39 55	—	—	0.048	11	A4059

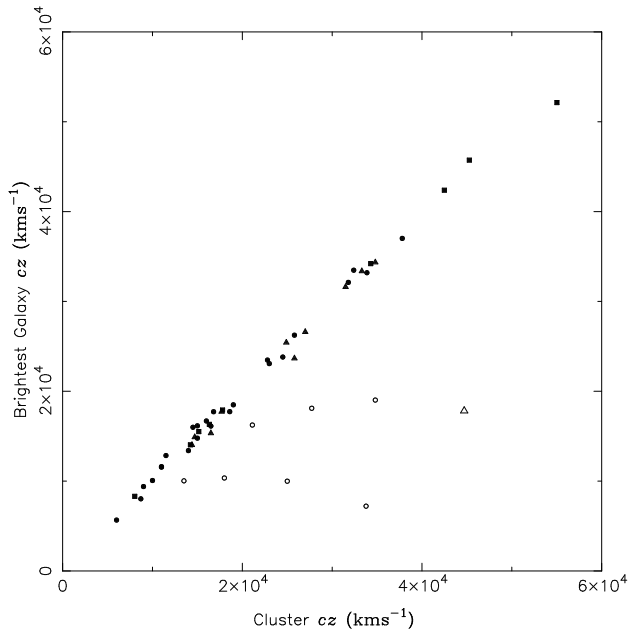


Figure 7. The redshifts of the brightest galaxies in cluster fields relative to the true cluster redshifts. The data shown are from Colless & Hewett (1987) (triangles), Teague, Carter & Gray (1990) (squares) and this work (circles). Open symbols show those points which were rejected by the likelihood ratio test as described in § 3.

In many cases this procedure allowed observations for more than two galaxies per cluster subject to the constraint of possible slit alignments.

We obtained redshifts for 141 clusters at the AAT in four nights in November of 1990, using the RGO spectrograph, 600V grating, and IPCS, giving 2048 bins in the wavelength direction with a resolution of $\sim 1\text{\AA}/\text{pixel}$ in the range 3670–5680 \AA and a useable slit length of 3.5'. Sample spectra, showing the absorption and emission features used to determine the redshifts are shown in figure 8. redshifts for a further 32 clusters were obtained by Jon Loveday using the Mt. Stromlo 2.3m telescope. Before observing we cross-referenced our list of target galaxies with Huchra (1990), which gave another 5 cluster redshifts. A further four redshifts were rejected by the maximum likelihood analysis, showing that carefully selecting the galaxies to be observed gives a significant improvement over simply selecting the brightest galaxy in the cluster field independently of position relative to the cluster centre.

In table 3 we list the galaxy redshifts for each cluster, together with the maximum likelihood redshift estimate, and the probability for the observed galaxy to be a cluster member. The numbers in columns 3 and 4 refer to the whole magnitude distribution of the cluster field. We also checked each likelihood interactively to remove any possible contamination from bright galaxies. Where changes were necessary the adopted values of the maximum likelihood redshift and probability for cluster membership are given in columns 5 and 6.

In §3 we assumed that the luminosity function for galaxies in clusters was the same as that for the field. We tested this assumption by changing the input luminosity function parameters to

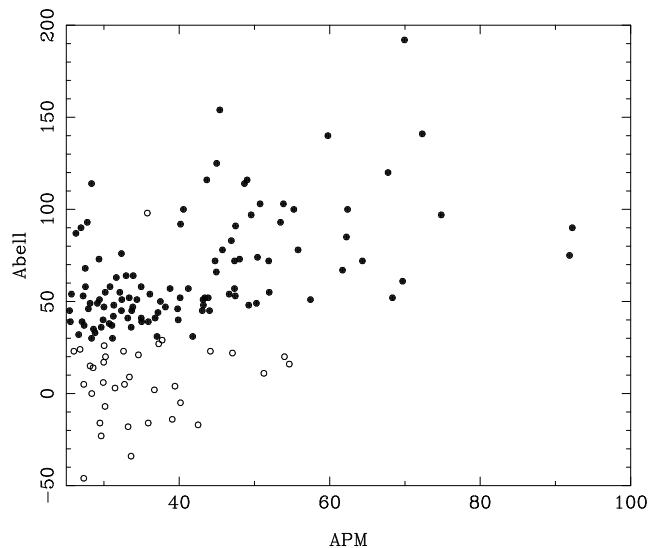


Figure 10. A comparison of our richness estimates, \mathcal{R} , with the Abell counts for clusters with Abell identifications in Table 4. Open circles denote supplementary Abell clusters.

$$B_{J^*} = -20.05; \quad \alpha = -1.25,$$

consistent with the findings of Rhee (1989), Colless (1989), and with our own internal estimates based on this sample of clusters (*in preparation*). We find that the changes in the likelihood estimates obtained in this way are within the original error estimates, and that repeating the interactive analysis with these parameters produces no change to our cluster redshift list.

The cluster redshift list is given in Table 4. The distribution of our survey in redshift-space is shown in figure 9. Where the centre of an Abell cluster lies within the counting circle of an APM cluster we give the Abell identification, although in some cases our use of a small defining radius means that an Abell cluster will be identified as more than one APM cluster. Fig. 10 shows a large scatter between our richness measure, \mathcal{R} and the Abell richness listed by Abell, Corwin & Olowin's (1989). We note that a considerable number of our clusters identify with the supplementary clusters of ACO. This is not surprising given the large scatter in the Abell richness counts (see also Lumsden *et al.* 1992). A more detailed comparison between our catalog and the ACO catalog, with a discussion of possible error mechanisms within the Abell catalogues will be given in a future paper.

6 SUMMARY

We have selected a catalogue of rich galaxy clusters from the APM Galaxy Survey using uniform selection criteria. Using redshifts from the literature and a small number of multi-fibre observations we have optimised our observing strategy and obtained a large, complete sample of cluster redshifts by making only one single-slit observation of most of our clusters. Foreground redshifts have been removed from the final sample by using a maximum likelihood analysis of the APM data for each cluster field. The two-point correlation function for this sample has been discussed by Dalton *et al.*

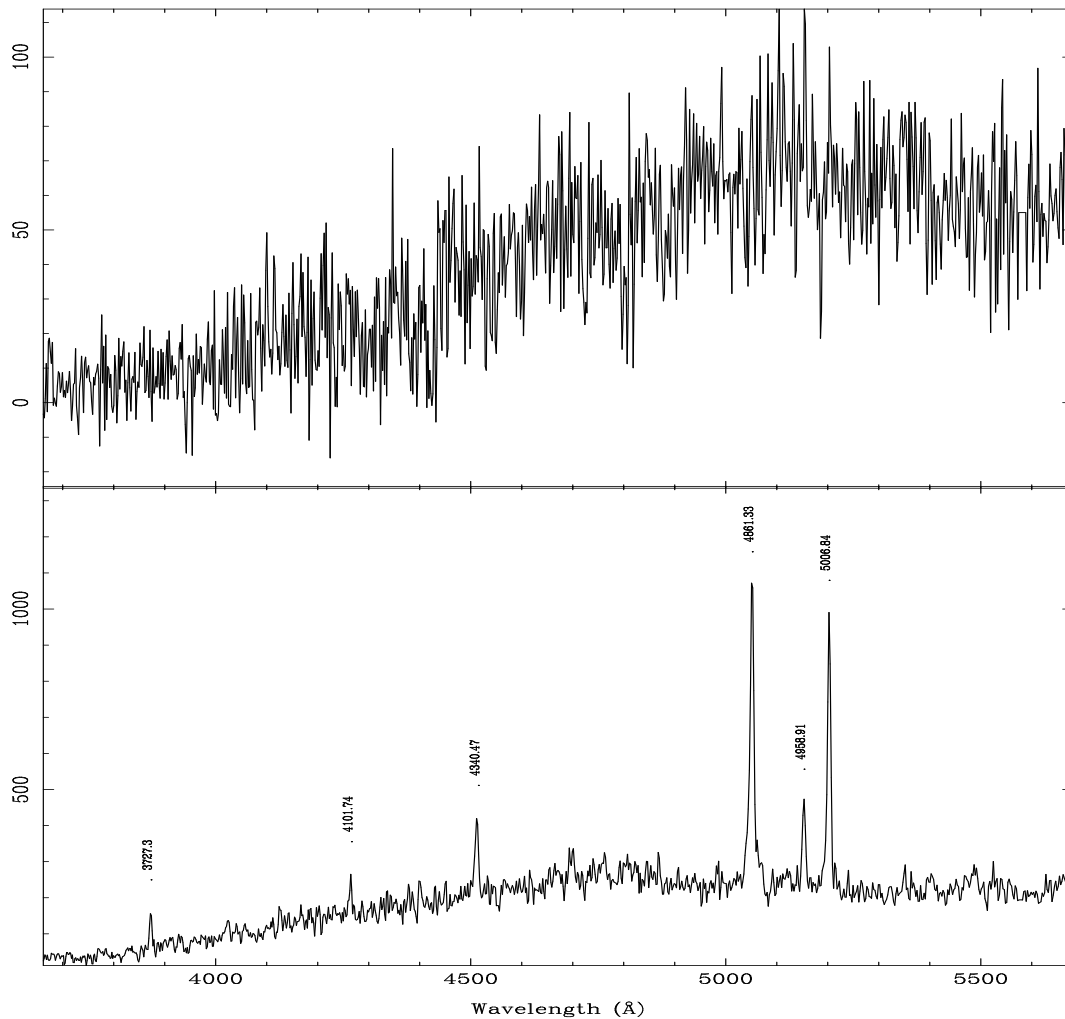


Figure 8. Typical spectra showing the absorption, and emission features used for redshift determinations.

(1992), and a comparison of the clustering properties of this sample with redshift samples of Abell clusters has been presented by Efstathiou *et al.* (1992).

An extension of the redshift survey is currently in progress, with the intention of obtaining redshifts for over 500 rich clusters using similar techniques to those described here. We will discuss the extension, together with modifications of the cluster finding algorithm and detailed comparisons with the Abell catalogue in future papers.

7 ACKNOWLEDGEMENTS

We would like to thank the staff of the Anglo-Australian Telescope, particularly Ray Sharples for technical assistance with AUTOFIB, and Max Pettini for observing support. This work has been supported by grants from the UK Science and Engineering Research Council. G.B.D acknowledges the receipt of an SERC studentship and travel grants in support of this work.

References

- Abell, G. O., Corwin, H. C. & Olowin, R. P., 1989. *Ap. J. Suppl.*, **70**, 1.
- Abell, G. O., 1958. *Ap. J. Suppl.*, **3**, 211.
- Andernach, H., 1989. *preprint*, .
- Colless, M. & Hewett, P., 1987. *Mon. Not. R. astr. Soc.*, **224**, 453.
- Colless, M., 1989. *Mon. Not. R. astr. Soc.*, **237**, 799.
- Dalton, G. B., Efstathiou, G., Maddox, S. J. & Sutherland, W. J., 1992. *Ap. J. Lett.*, **390**, L1.
- Dekel, A., Blumenthal, G. R., Primack, J. R. & Olivier, S., 1989. *Ap. J. Lett.*, **338**, L5.
- Efstathiou, G., Dalton, G. B., Sutherland, W. J. & Maddox, S. J., 1992. *Mon. Not. R. astr. Soc.*, **257**, 125.
- Huchra, J. P., 1990. *Private communication*, .

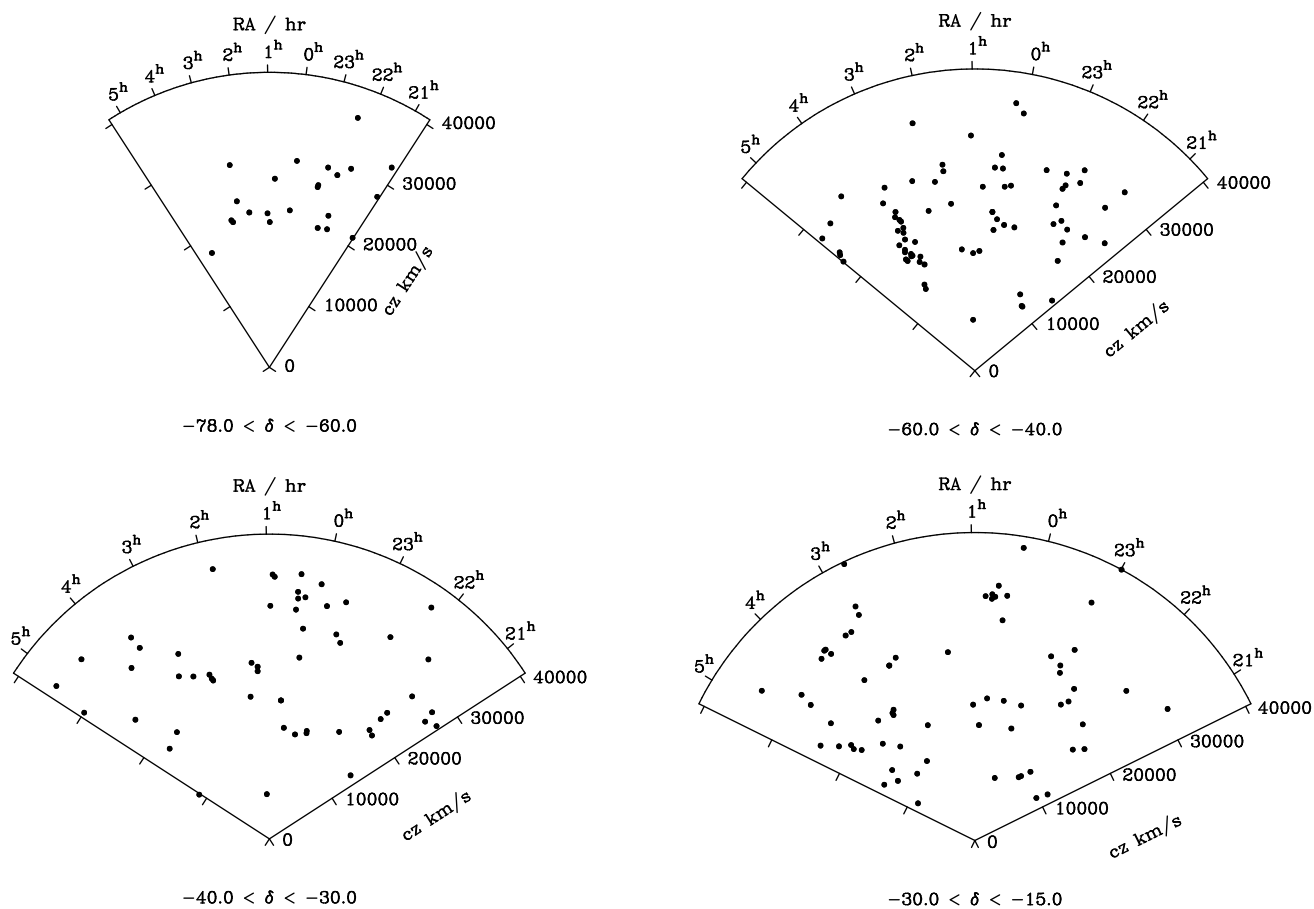


Figure 9. The sky distribution of the survey. The large structure seen at $\alpha = 3$ hours is the Horologium-Reticulum supercluster.

Lilje, P. B. & Efstathiou, G., 1988. *Mon. Not. R. astr. Soc.*, **231**, 635.

Loveday, J., Peterson, B. A., Efstathiou, G. & Maddox, S. J., 1992. *Ap. J.*, **390**, 338.

Lumsden, S. L., Nichol, R. C., Collins, C. A. & Guzzo, L., 1992. *Mon. Not. R. astr. Soc.*, **258**, 1.

Maddox, S. J., Efstathiou, G. & Sutherland, W. J., 1990b. *Mon. Not. R. astr. Soc.*, **246**, 433.

Maddox, S. J., Efstathiou, G. & Sutherland, W. J., 1993. *Mon. Not. R. astr. Soc.*, , in preparation.

Maddox, S. J., Sutherland, W. J., Efstathiou, G. & Loveday, J., 1990a. *Mon. Not. R. astr. Soc.*, **243**, 692.

Peacock, J. A. & West, M. J., 1992. *Mon. Not. R. astr. Soc.*, **259**, 494.

Rhee, G. F. R. N., 1989. *PhD thesis*, Leiden University.

Sutherland, W. J. & Efstathiou, G., 1991. *Mon. Not. R. astr. Soc.*, **248**, 159.

Sutherland, W. J., 1988. *Mon. Not. R. astr. Soc.*, **234**, 159.

Teague, P. F., Carter, D. & Gray, P. M., 1990. *Ap. J. Suppl.*, **72**, 715.

Tonry, J. & Davis, M., 1979. *Ap. J.*, **84**, 1511.

West, R. M. & Fransden, S., 1981. *Astron. Astrophys. Suppl.*, **44**, 329.

Zwicky, F., Herzog, E., Wild, P., Karpowicz, M. & Kowal, C. T., 1968. *Catalogue of Galaxies and Clusters of Galaxies*, California Institute of Technology, Pasadena.

Table 3. Redshifts for galaxies in clusters observed using a single slit. Entries in columns (5) and (6) only occur for those fields where an interactive application of the analysis changed the redshift of maximum likelihood (see text).

(1) Cluster	(2) z_{obs}	(3) $z_{\mathcal{L}}$	(4) P	(5) $z_{\mathcal{L}int}$	(6) P_{int}
0001-5103	0.0393	0.1419	0.002*		
0001-5103	0.1179	0.1213	0.81	0.1179	1.00
0008-2908	0.0602	0.0555	0.5708		
0008-2908	0.0646	0.0543	0.3090*		
0009-4232	0.0860	0.0908	0.84	0.0911	0.42
0009-4232	0.0860	0.0956	0.50	0.0907	0.69
0011-4317	0.1199	0.0821	0.0998*	0.1027	0.4114
0011-4317	0.1234	0.0773	0.0664*	0.0986	0.2690*
0013-3136	0.0719	0.0981	0.6439		
0013-3136	0.0805	0.1020	0.5557		
0013-4850	0.0677	0.0497	0.41	0.0821	0.54
0013-4850	0.0699	0.0531	0.53	0.0923	0.40
0013-4850	0.0700	0.0531	0.53	0.0925	0.38
0015-3526	0.0903	0.0803	0.30*	0.0877	0.73
0015-3526	0.0946	0.0801	0.15*	0.0895	0.41
0015-3526	0.0948	0.0802	0.15*	0.0895	0.41
0018-3413	0.1069	0.1039	0.83		
0018-3413	0.1087	0.1025	0.69		
0018-3413	0.1088	0.1026	0.69		
0018-3413	0.1103	0.1009	0.61		
0020-5353	0.0966	0.1020	0.73		
0020-5353	0.0985	0.1040	0.69		
0024-4849	0.0720	0.1030	0.4206		
0024-4907	0.0710	0.0939	0.25*	0.0939	0.39
0024-4907	0.0722	0.0955	0.27*	0.0955	0.40
0025-3033	0.1135	0.1200	0.83	0.1200	0.68
0025-3033	0.1192	0.1192	1.00	0.1209	0.90
0025-3542	0.1067	0.1097	0.86		
0025-3542	0.1076	0.1076	1.00		
0025-3542	0.1078	0.1078	1.00		
0026-3032	0.0744	0.0985	0.16*		
0026-3032	0.1032	0.1061	0.87		
0026-3516	0.1106	0.1043	0.50	0.1156	0.69
0026-3516	0.1109	0.1014	0.46	0.1156	0.69
0027-2944	0.0657	0.0831	0.3689		
0027-2944	0.0972	0.0808	0.3546		
0027-2944	0.0979	0.0787	0.3293		
0027-5341	0.0862	0.1100	0.04*		
0027-5341	0.0864	0.1103	0.04*		
0027-5341	0.0921	0.1075	0.16*	0.1023	0.34
0035-3107	0.0606	0.1365	0.000*	†	
0035-3107	0.0622	0.1340	0.001*	†	
0035-3107	0.0626	0.1349	0.001*	†	
0035-3924	0.0622	0.0622	1.00		
0035-3924	0.0623	0.0623	1.00		
0035-3924	0.0633	0.0666	0.66		
0036-2234	0.0631	0.0565	0.6335		
0036-2234	0.0645	0.0577	0.6027		
0037-2625	0.0759	0.1089	0.3007*	0.1007	0.4425
0040-2621	0.1067	0.0901	0.24*	0.1052	0.88
0040-2621	0.1089	0.0904	0.19*	0.1058	0.78
0040-2621	0.1115	0.0956	0.25*	0.1083	0.78
0040-2852	0.1069	0.0902	0.23*	0.0978	0.43
0040-2852	0.1094	0.0877	0.14*		
0043-6351	0.0746	0.0807	0.35	0.0826	0.24*
0043-6351	0.0750	0.0791	0.43	0.0811	0.29*
0043-6351	0.0866	0.0794	0.28*	0.0806	0.34

Table 3. (*continued*)

(1) Cluster	(2) z_{obs}	(3) $z_{\mathcal{L}}$	(4) P	(5) $z_{\mathcal{L}int}$	(6) P_{int}
0044-5500	0.0811	0.0855	0.67		
0044-5500	0.0830	0.0853	0.76		
0045-6334	0.0305	0.1074	0.00*	0.1123	0.00*
0045-6334	0.0593	0.0963	0.01*	0.1086	0.001*
0046-4215	0.0533	0.1507	0.02*	0.0587	0.63
0046-4215	0.0537	0.2667	0.01*	0.0592	0.60
0048-2846	0.0510	0.1125	0.00*	0.0664	0.33
0048-2846	0.0550	0.1113	0.00*	0.0662	0.50
0051-3117	0.0287	0.0287	1.00	0.1070	0.00*
0051-3117	0.1170	0.1070	0.62		
0054-3809	0.1154	0.1022	0.52		
0054-3809	0.1175	0.1007	0.46		
0056-3432	0.0878	0.1267	0.0710*		
0056-3432	0.1040	0.1267	0.3619		
0056-6704	0.0663	0.0857	0.23*	0.0734	0.52
0056-6704	0.0683	0.0829	0.19*	0.0756	0.35
0101-4307	0.0506	0.0519	0.84		
0101-4307	0.0548	0.0548	1.00		
0102-6710	0.0697	0.0660	0.80	0.0697	1.00
0102-6710	0.0706	0.0668	0.78	0.0687	0.85
0115-3650	0.0734	0.1130	0.20*		
0115-3650	0.0752	0.1119	0.32*		
0115-3815	0.0772	0.0772	1.00		
0115-3815	0.0773	0.0773	1.00		
0115-3815	0.1189	0.0730	0.03*		
0124-3810	0.0773	0.1046	0.02*	0.0941	0.33
0124-3810	0.0807	0.1028	0.06*	0.0939	0.46
0131-2714	0.0821	0.1182	0.17*		
0131-2714	0.0838	0.1207	0.20*		
0132-2740	0.0869	0.1782	0.00*		
0132-2740	0.0873	0.1791	0.00*		
0132-3305	0.0638	0.0571	0.73	0.0722	0.47
0132-3305	0.0646	0.0492	0.58	0.0714	0.56
0144-5539	0.0944	0.0918	0.82		
0144-5539	0.1346	0.0879	0.004*		
0144-5618	0.0906	0.1284	0.08*		
0144-5618	0.0920	0.1330	0.09*		
0152-3555	0.0334	0.1270	0.001*		
0152-3555	0.1228	0.1158	0.67		
0156-6438	0.0696	0.0938	0.11*	0.0845	0.35
0156-6438	0.0735	0.0933	0.18*	0.0893	0.42
0159-4829	0.0853	0.0924	0.56		
0159-4829	0.0873	0.0873	1.00		
0221-4840	0.0738	0.0698	0.84		
0221-4840	0.0747	0.0707	0.81		
0225-6714	0.0942	0.1179	0.17*	0.1152	0.51
0225-6714	0.0968	0.1185	0.20*	0.1076	0.59
0225-6956	0.0772	0.0793	0.90	0.0856	0.65
0225-6956	0.0781	0.0781	1.00	0.0868	0.67
0227-3404	0.0730	0.0966	0.24*		
0227-3404	0.0751	0.0975	0.24*		
0227-3404	0.0810	0.0987	0.35		
0229-2311	0.0550	0.0550	1.00	0.055	1.00
0229-2311	0.0557	0.0557	1.00	0.0557	1.00
0229-2311	0.0573	0.0573	1.00	0.0573	1.00
0229-3215	0.0767	0.0934	0.20*	0.0892	0.60
0229-3215	0.0780	0.0993	0.20*	0.0949	0.41

Table 3. (continued)

(1) Cluster	(2) z_{obs}	(3) $z_{\mathcal{L}}$	(4) P	(5) $z_{\mathcal{L}int}$	(6) P_{int}
0232-5948	0.0877	0.1023	0.31*		
0232-5948	0.0905	0.1006	0.44		
0234-1934	0.0861	0.0932	0.49		
0234-1934	0.0917	0.0917	1.00	0.1019	0.41
0242-2625	0.1350	0.0940	0.01*	0.1271	0.49
0242-2625	0.1464	0.0910	0.000*		
0245-1958	0.0858	0.0882	0.86		
0245-1958	0.0873	0.0873	1.00		
0245-2250	0.0838	0.0638	0.5066		
0245-2250	0.0857	0.0644	0.4514		
0245-2250	0.0859	0.0645	0.4491		
0245-2250	0.0884	0.0688	0.3867		
0249-2549	0.1117	0.1117	1.00		
0249-2549	0.1198	0.1061	0.59		
0249-7136	0.0676	0.1252	0.0564*		†
0249-7136	0.0689	0.1278	0.0622*		†
0249-7136	0.0705	0.1309	0.0413*		†
0253-3537	0.0794	0.0837	0.76	0.0924	0.53
0253-3537	0.0799	0.0843	0.78	0.0930	0.53
0253-3537	0.0815	0.0860	0.79	0.0949	0.53
0253-6636	0.0702	0.0740	0.75	0.0777	0.56
0253-6636	0.0714	0.0733	0.84	0.0791	0.60
0258-3638	0.0494	0.0691	0.17*		
0258-3638	0.0917	0.0777	0.49	0.0935	0.70
0258-3638	0.0958	0.0770	0.36	0.0958	1.00
0304-1752	0.1062	0.1212	0.40	0.1182	0.12*
0304-1752	0.1062	0.1212	0.40	0.1182	0.12*
0304-1752	0.1069	0.1190	0.43	0.1159	0.64
0307-4727	0.0626	0.0922	0.0586*	0.0791	0.3866
0307-4727	0.0638	0.0907	0.0912*	0.0726	0.4832
0309-2707	0.0684	0.0684	1.00		
0309-2707	0.0684	0.0684	1.00		
0309-2707	0.1664	0.0491	0.00*		
0310-2721	0.0643	0.0575	0.5630		
0310-2721	0.0646	0.0646	1.00		
0310-2721	0.1074	0.0557	0.0398*		
0310-2721	0.1080	0.0682	0.07*		
0310-5305	0.0570	0.1862	0.0005*		†
0311-3829	0.0798	0.1016	0.15*		
0311-3829	0.0847	0.1010	0.28*	0.1034	0.39
0313-1917	0.0657	0.0936	0.15*	0.0831	0.34
0313-1917	0.0676	0.0892	0.20*	0.0819	0.40
0313-2926	0.0641	0.0607	0.7553		
0313-2926	0.0670	0.0598	0.5888		
0314-4406	0.0916	0.0865	0.7203		
0315-4442	0.0760	0.0884	0.27*	0.0842	0.38
0315-4442	0.1287	0.1064	0.26*		
0316-4551	0.0766	0.0766	1.00		
0316-4551	0.0767	0.0767	1.00		
0316-4551	0.0808	0.0808	1.00		
0316-4551	0.0821	0.0776	0.71		
0320-2459	0.0857	0.1330	0.07*		†
0320-2459	0.0871	0.1305	0.07*		†
0320-2459	0.0884	0.1276	0.09*		†
0320-4544	0.0670	0.0706	0.78		
0320-4544	0.0696	0.0733	0.76		
0320-4544	0.0717	0.0717	1.00		

Table 3. (continued)

(1) Cluster	(2) z_{obs}	(3) $z_{\mathcal{L}}$	(4) P	(5) $z_{\mathcal{L}int}$	(6) P_{int}
0320-5320	0.0768	0.0664	0.50		0.0872
0320-5320	0.0769	0.0664	0.49		0.0874
0320-5320	0.0798	0.0645	0.33		0.0863
0320-5320	0.0798	0.0645	0.33		0.0863
0320-5320	0.0799	0.0646	0.33		0.0843
0323-5845	0.0655	0.0620	0.73		
0323-5845	0.0684	0.0611	0.57		
0327-4610	0.0702	0.0627	0.49		
0327-4610	0.0720	0.0623	0.36		
0333-2900	0.0423	0.0423	1.00	0.1071	0.00*
0333-2900	0.1037	0.1037	1.00		
0334-2812	0.1052	0.0903	0.40	0.0874	0.39
0334-2812	0.1068	0.0947	0.48	0.0917	0.35
0334-2812	0.1486	0.0836	0.003*		
0334-5350	0.0622	0.0622	1.00		
0334-5350	0.0627	0.0627	1.00		
0335-3957	0.0674	0.0961	0.06*		
0335-3957	0.0683	0.0975	0.07*		
0335-3957	0.1034	0.0946	0.51	0.0990	0.66
0336-2510	0.0507	0.0507	1.00	0.0557	0.65
0336-2510	0.0533	0.0533	1.00	0.0534	1.00
0336-2510	0.0534	0.0534	1.00	0.0534	1.00
0336-2843	0.1071	0.1071	1.00		
0336-2843	0.1074	0.1074	1.00		
0336-3319	0.1088	0.1026	0.75		
0336-3319	0.1116	0.1116	1.00		
0336-4045	0.0620	0.0944	0.3750		
0338-2850	0.0658	0.0606	0.54	0.0658	1.00
0338-2850	0.0685	0.0612	0.39	0.0667	0.79
0339-4551	0.0661	0.0801	0.07*	0.0765	0.36
0339-4551	0.0670	0.0830	0.08*	0.0741	0.42
0343-4123	0.0536	0.0754	0.11*	0.0645	0.37
0343-4123	0.0589	0.0711	0.31*	0.0650	0.60
0345-1748	0.0233	0.1563	0.00*		
0345-1748	0.1486	0.1486	1.00		
0346-1807	0.0376	0.1618	0.00*	0.1618	†
0346-1807	0.0386	0.1601	0.00*	0.1601	†
0356-3021	0.0926	0.1003	0.50		
0356-3021	0.0932	0.1010	0.47		
0356-3021	0.0971	0.0998	0.73		
0356-3021	0.0980	0.1008	0.77		
0357-2439	0.0580	0.0580	1.00	0.0802	0.57
0357-2439	0.0592	0.0838	0.66	0.0802	0.57
0406-3105	0.0569	0.0803	0.002*		
0406-3105	0.0635	0.0785	0.05*	0.0701	0.49
0406-3105	0.1150	0.0789	0.002*		
0412-5507	0.0990	0.0990	1.00		
0412-5507	0.0990	0.0990	1.00		
0412-5507	0.0990	0.0990	1.00		
0422-2752	0.0462	0.0462	1.00		
0422-2752	0.0471	0.0471	1.00		
0422-2752	0.0484	0.0484	1.00		
0424-2842	0.0977	0.1087	0.23*	0.1086	0.33
0424-2842	0.1001	0.1114	0.32*	0.1085	0.46
0426-2821	0.0940	0.0468	0.05*		
0426-2821	0.0950	0.0472	0.05*		
0426-2821	0.0952	0.0473	0.05*		

Table 3. (*continued*)

(1)	(2)	(3)	(4)	(5)	(6)
Cluster	z_{obs}	$z_{\mathcal{L}}$	P	$z_{\mathcal{L}int}$	P_{int}
0427-1742	0.0795	0.0665	0.46		
0427-1742	0.0816	0.0682	0.42		
0427-1742	0.0829	0.0692	0.40		
0430-2111	0.0639	0.1683	0.000*	0.1683	†
0430-2111	0.0647	0.1673	0.000*	0.1673	†
0431-3246	0.1162	0.0963	0.12*		
0431-3246	0.1179	0.0943	0.08*		
0433-2835	0.0433	0.0641	0.04*	0.0579	0.36
0433-2835	0.0433	0.0641	0.04*	0.0579	0.36
0434-2232	0.0319	0.0593	0.31*		
0434-2232	0.0690	0.0653	0.77		
0438-3539	0.0594	0.0285	0.10*	0.0594	1.00
0438-3539	0.0597	0.0286	0.09*	0.0597	1.00
0440-3252	0.0434	0.1227	0.00*		
0440-3252	0.0799	0.0799	1.00		
0444-2534	0.1150	0.1035	0.37		
0449-5112	0.0914	0.1219	0.12*	0.1016	0.30*
0449-5112	0.0914	0.1219	0.12*	0.1016	0.41
0449-5112	0.0921	0.1255	0.11*	0.1023	0.43
0459-1808	0.0577	0.0994	0.01*	0.1054	0.004*
0459-1822	0.0427	0.0958	0.00*		
0459-1822	0.0430	0.0966	0.00*		
0459-1822	0.0797	0.0819	0.78		
0459-1822	0.0800	0.0822	0.79		
0508-3611	0.1168	0.1051	0.34	0.1155	0.70
0508-3611	0.1190	0.1062	0.31*	0.1155	0.70
0512-4147	0.0785	0.1106	0.02*	0.0956	0.32
0512-4147	0.0813	0.1080	0.04*	0.0991	0.39
0513-4907	0.0564	0.1057	0.00*		
0513-4907	0.0913	0.1040	0.22*	0.1016	0.38
0513-4907	0.0914	0.1041	0.22*	0.1016	0.38
0513-4907	0.0939	0.1044	0.30*	0.1018	0.47
0513-4907	0.0944	0.1050	0.31*	0.1023	0.49
0514-3508	0.0996	0.1248	0.22*	0.1220	0.33
0514-3508	0.1004	0.1286	0.20*	0.1230	0.32
0515-4211	0.0803	0.1242	0.01*	0.1154	0.36
0519-4054	0.0709	0.1052	0.04*	0.0861	0.48
0519-4054	0.0770	0.1021	0.14*	0.0854	0.64
0523-3131	0.0314	0.0314	1.00	0.0374	1.00
0523-3131	0.0374	0.0323	0.42	0.0374	1.00
2038-6135	0.0927	0.0539	0.10*	0.0953	0.82
2045-6211	0.1058	0.0848	0.27*		
2045-6211	0.1100	0.0850	0.19*	0.0975	0.32*
2052-3610	0.0869	0.1638	0.19*	0.1638	†
2056-3536	0.0918	0.1020	0.5534		
2056-3536	0.0918	0.1020	0.5534		
2057-4422	0.1426	0.0991	0.07*	0.1426	1.00
2057-4422	0.1431	0.1015	0.06*	0.1431	1.00
2102-3859	0.1487	0.1660	0.34		
2102-3859	0.1554	0.1736	0.50		
2106-2716	0.0862	0.0910	0.8196		
2106-2716	0.1030	0.1030	1.0000		
2128-4330	0.1047	0.1047	1.00		
2128-4330	0.1047	0.1047	1.00		
2128-4330	0.1050	0.1050	1.00		
2129-2411	0.0626	0.1053	0.03*		†
2129-2411	0.0644	0.1052	0.04*		†

Table 3. (*continued*)

(1)	(2)	(3)	(4)	(5)	(6)
Cluster	z_{obs}	$z_{\mathcal{L}}$	P	$z_{\mathcal{L}int}$	P_{int}
2129-3525	0.0898	0.1048	0.45		
2129-3525	0.0901	0.1001	0.51		
2130-3128	0.0648	0.0665	0.82		
2130-3128	0.0656	0.0656	1.00		
2135-5141	0.0588	0.0832	0.1470*		
2135-5141	0.0936	0.0832	0.5391		
2138-3413	0.0764	0.0847	0.6172		
2138-3413	0.0780	0.0865	0.6617		
2139-3309	0.0726	0.0726	1.0000		
2139-3309	0.0739	0.0739	1.0000		
2140-3914	0.0658	0.0920	0.07*	0.0799	0.41
2140-3914	0.0663	0.0909	0.08*	0.0799	0.41
2142-2010	0.0577	0.1054	0.001*	0.0830	0.46
2142-2010	0.0587	0.1044	0.001*	0.0830	0.46
2144-4407	0.0605	0.0605	1.00		
2144-4407	0.0639	0.0706	0.38	0.0706	0.38
2145-3251	0.0851	0.1063	0.3202		
2145-3251	0.1066	0.1066	1.0000		
2155-7206	0.0690	0.1427	0.0137		†
2157-4324	0.0667	0.0950	0.07*	0.0809	0.52
2157-4324	0.0750	0.1034	0.13*	0.0830	0.62
2203-4600	0.0690	0.0985	0.11*		
2203-4600	0.0743	0.0984	0.21*	0.0824	0.71
2203-4600	0.0782	0.0974	0.29*	0.0824	0.79
2203-4600	0.0935	0.0935	1.00		
2207-6546	0.0193	0.1123	0.000*	0.1220	0.00*
2207-6546	0.0746	0.1069	0.16*	0.0706	0.77
2211-3658	0.0330	0.1595	0.00*		
2211-3658	0.0334	0.1563	0.00*		
2215-2428	0.0387	0.0530	0.10*	0.0478	0.52
2215-2428	0.0388	0.0532	0.10*	0.0478	0.52
2220-5528	0.0782	0.0952	0.26*	0.0952	0.43
2220-5528	0.0783	0.0954	0.27*	0.0954	0.43
2221-6152	0.0869	0.1253	0.02*		
2221-6152	0.1221	0.1221	1.00		
2224-4909	0.0973	0.0918	0.53		
2224-4909	0.0973	0.0918	0.53		
2224-4909	0.1009	0.0910	0.39		
2224-6916	0.0646	0.0680	0.7812		
2224-6916	0.0658	0.0658	1.0000		
2224-6916	0.0678	0.0678	1.0000		
2227-4825	0.1019	0.0890	0.35		
2227-4825	0.1025	0.0895	0.34		
2227-4825	0.1035	0.0889	0.30*		
2229-2541	0.0336	0.0336	1.0000		
2229-2541	0.0363	0.0363	1.0000		
2233-2435	0.0312	0.0365	0.41	0.0392	0.40
2233-2435	0.0342	0.0342	1.00	0.0342	1.00
2236-1736	0.0727	0.1041	0.04*	0.0837	0.34
2236-1736	0.0740	0.0980	0.06*	0.09	0.37
2239-2515	0.0800	0.0712	0.6423		
2240-5928	0.0828	0.1056	0.40		
2240-5928	0.0830	0.1058	0.39		
2241-4547	0.0449	0.0798	0.02*		
2241-4547	0.0934	0.0882	0.73		
2242-4610	0.0886	0.1279	0.01*	0.0885	1.00
2242-4610	0.0908	0.1312	0.01*	0.1009	0.52

Table 3. (continued)

(1) Cluster	(2) z_{obs}	(3) $z_{\mathcal{L}}$	(4) P	(5) $z_{\mathcal{L}int}$	(6) P_{int}
2243-1757	0.0707	0.0802	0.42		
2243-1757	0.0731	0.0790	0.58		
2246-5203	0.0950	0.1056	0.43	0.1056	0.55
2246-5203	0.0999	0.1055	0.70	0.1046	0.67
2246-6439	0.0937	0.0989	0.70		
2246-6439	0.0969	0.0969	1.00		
2256-6853	0.0847	0.1034	0.45	0.0940	0.53
2256-6853	0.0889	0.1012	0.60	0.0938	0.76
2257-6154	0.0843	0.1075	0.37	0.1075	0.33
2257-6154	0.0882	0.1077	0.44	0.1077	0.48
2309-2920	0.0863	0.1149	0.09*		
2309-2920	0.1169	0.1136	0.82		
2314-3913	0.0629	0.1158	0.16*		
2314-4258	0.0958	0.1119	0.48	0.1172	0.40
2324-2407	0.0876	0.0973	0.48	0.0997	0.37
2324-2407	0.0887	0.0961	0.56	0.1009	0.35
2325-3639	0.0636	0.0603	0.8087*	0.1038	0.0699*
2325-3639	0.0939	0.0572	0.1035*	0.1044	0.6615
2325-3639	0.0944	0.0575	0.1018*	0.1050	0.6655
2329-3424	0.0505	0.0910	0.001*	0.0606	0.44
2329-3424	0.0514	0.0928	0.001*	0.0617	0.41
2333-3614	0.0960	0.0960	1.00		
2333-3614	0.0964	0.0964	1.00		
2334-3300	0.1095	0.1095	1.00		
2334-3300	0.1109	0.1109	1.00		
2336-4615	0.0671	0.0778	0.56		
2338-2928	0.0624	0.0689	0.47		
2338-2928	0.0628	0.0694	0.49		
2342-2614	0.0513	0.0565	0.69	0.0616	0.46
2342-2614	0.0517	0.0569	0.69	0.0621	0.44
2353-3353	0.1050	0.0783	0.25*	0.0924	0.37
2353-3353	0.1070	0.0797	0.22*	0.0949	0.33
2357-6647	0.0730	0.1242	0.1789*	0.1045	0.3579
2358-4950	0.0662	0.0662	1.0000		
2358-4950	0.0671	0.0671	1.0000		
2359-5418	0.0850	0.0944	0.6997		

Notes:

- * This galaxy is rejected on the basis of the likelihood ratio test.
- † The likelihood function for this cluster is unstable. If the galaxy redshifts agree then this is adopted as the cluster redshift.

Table 4. Cluster redshifts obtained using the likelihood ratio test.

(1) $\alpha(1950)$	(2) $\delta(1950)$	(3) m_X	(4) \mathcal{R}	(5) z	(6) Abell
00 01 04.10	-51 03 33.12	18.536	56.173	0.118 ¹	
00 03 43.51	-34 59 05.27	19.083	69.943	0.116 ³	A2721
00 08 58.03	-29 08 11.40	17.700	27.547	0.063 ²	A2734
00 09 18.96	-42 32 31.20	18.447	33.174	0.084 ¹	A2736
00 11 23.50	-43 17 15.72	17.582	27.308	0.122 ²	
00 13 53.78	-48 50 58.20	18.746	30.123	0.069 ¹	
00 13 56.11	-31 36 33.12	18.705	27.515	0.082 ²	A2751
00 15 14.45	-35 26 09.60	18.621	67.754	0.095 ¹	A2755
00 16 05.71	-42 02 58.56	18.169	27.368	0.092 ¹	A2758
00 18 01.94	-49 33 47.53	17.608	30.170	0.064 ³	A2764
00 18 04.13	-25 58 36.48	19.396	72.301	0.131 ³	A0022
00 18 06.26	-34 13 24.95	18.796	45.214	0.109 ¹	
00 20 04.99	-53 53 36.60	18.612	35.719	0.098 ¹	
00 23 00.67	-33 19 18.12	16.701	30.030	0.050 ³	S0041
00 24 19.63	-48 49 05.52	18.529	27.640	0.072 ²	
00 24 29.52	-49 07 45.48	18.187	36.167	0.072 ¹	
00 25 16.90	-30 33 15.48	18.547	34.386	0.119 ¹	A2778
00 25 41.54	-35 42 29.51	18.568	39.551	0.108 ¹	
00 26 07.54	-23 53 19.32	19.227	45.402	0.109 ³	A0042
00 26 39.36	-35 16 05.52	18.687	39.311	0.111 ¹	
00 26 41.47	-30 32 44.16	18.262	29.409	0.103 ¹	A2778
00 27 42.31	-29 44 35.16	17.836	27.238	0.098 ²	A2784
00 27 53.04	-53 41 09.60	18.314	43.219	0.092 ¹	A2782
00 35 05.52	-39 24 52.20	18.443	31.646	0.062 ¹	A2799
00 35 16.63	-31 07 06.96	18.675	41.214	0.062 ¹	A2794
00 36 55.87	-22 34 12.72	17.127	28.157	0.063 ²	A0074
00 37 26.69	-26 25 08.40	18.392	32.296	0.108 ²	
00 40 30.62	-26 21 03.24	17.321	31.969	0.109 ¹	
00 40 34.94	-28 52 22.44	18.589	40.127	0.107 ¹	A2814
00 43 56.78	-63 51 35.65	18.406	92.237	0.087 ¹	A2819
00 44 31.01	-55 00 37.44	17.700	37.740	0.083 ¹	S0077
00 46 07.15	-42 15 52.93	18.131	28.039	0.054 ¹	
00 48 54.96	-28 46 19.92	18.503	37.505	0.051 ¹	A2829
00 51 53.81	-31 17 35.52	17.989	29.943	0.117 ¹	
00 54 03.70	-38 09 56.87	18.713	33.606	0.118 ¹	S0106
00 56 01.63	-67 04 17.05	17.747	54.633	0.067 ¹	S0112
00 56 09.38	-34 32 20.41	18.835	30.811	0.104 ²	A2847
01 00 19.56	-22 09 07.92	17.988	38.168	0.060 ³	A0133
01 01 49.25	-43 07 31.44	17.784	35.768	0.053 ¹	S0121
01 02 45.82	-67 10 53.03	17.781	35.014	0.071 ¹	A2864
01 07 40.08	-46 10 28.56	15.983	31.139	0.023 ³	A2877
01 15 18.62	-38 15 43.20	17.911	38.790	0.077 ¹	A2891
01 15 44.74	-36 50 38.76	18.597	29.208	0.075 ¹	
01 24 03.14	-38 10 58.80	18.686	44.766	0.079 ¹	A2911
01 31 03.41	-27 14 19.68	18.069	29.129	0.084 ¹	A2924
01 32 06.53	-33 05 48.84	18.167	32.605	0.064 ¹	S0167
01 44 01.56	-55 39 09.71	18.094	36.684	0.094 ¹	
01 44 14.93	-56 18 07.56	17.732	32.842	0.091 ¹	
01 52 03.19	-35 55 08.40	18.765	43.067	0.123 ¹	A2952
01 56 21.50	-64 38 01.31	18.341	37.961	0.072 ¹	S0210
01 59 43.18	-48 29 44.88	18.042	30.151	0.087 ¹	S0218
02 04 06.67	-51 01 28.92	19.367	26.003	0.172 ⁴	S0222
02 11 07.32	-47 25 09.84	19.334	64.350	0.115 ⁴	A2988
02 21 35.38	-48 40 44.76	17.871	36.106	0.075 ¹	A3009
02 25 51.62	-67 14 53.16	18.139	33.617	0.095 ¹	A3021
02 25 53.35	-69 56 01.32	18.403	30.491	0.078 ¹	
02 27 21.19	-34 04 22.08	18.722	34.150	0.075 ¹	
02 29 16.75	-23 11 57.84	16.991	30.373	0.055 ¹	
02 29 51.91	-32 15 40.32	18.247	31.220	0.078 ¹	
02 32 50.45	-59 48 35.28	18.856	32.876	0.090 ¹	S0280
02 34 17.28	-19 34 56.64	18.692	47.352	0.088 ¹	A0367

Table 4. (*continued*)

(1) $\alpha(1950)$	(2) $\delta(1950)$	(3) m_X	(4) \mathcal{R}	(5) z	(6) Abell
02 42 04.42	-26 25 55.20	18.688	33.891	0.135 ¹	A0380
02 45 05.74	-19 58 51.60	18.340	31.446	0.086 ¹	
02 45 31.97	-22 50 38.76	18.171	27.184	0.086 ²	
02 49 15.29	-25 07 54.84	18.654	74.823	0.116 ³	A0389
02 49 38.28	-71 36 41.03	17.293	27.324	0.069 ²	S0303
02 49 59.98	-25 49 20.28	18.448	31.317	0.112 ¹	A3062
02 53 06.02	-35 37 58.08	17.902	28.754	0.080 ¹	
02 53 18.82	-66 36 44.63	17.941	28.159	0.070 ¹	S0311
02 58 23.45	-36 38 10.68	17.527	29.550	0.092 ¹	
03 04 13.01	-17 52 44.04	18.452	33.355	0.107 ¹	A0416
03 06 03.12	-23 52 49.44	—	—	0.041 ³	A0419
03 07 20.33	-47 27 25.20	17.942	27.789	0.064 ²	A3093
03 09 21.96	-27 07 36.12	18.319	50.267	0.068 ¹	A3095
03 10 27.94	-53 05 09.97	18.271	25.098	0.057 ²	
03 10 45.86	-27 21 34.20	17.940	30.697	0.107 ²	A3098
03 11 44.35	-38 29 29.05	18.620	48.196	0.083 ¹	
03 13 26.95	-29 26 30.12	17.442	26.832	0.067 ²	S0333
03 13 46.10	-19 17 35.88	17.636	30.004	0.066 ¹	A0428
03 14 30.41	-44 06 52.56	17.656	26.648	0.092 ²	A3109
03 14 51.84	-51 05 56.40	17.940	31.065	0.075 ³	A3110
03 15 55.32	-44 42 22.32	18.689	43.669	0.076 ¹	A3112
03 16 00.22	-45 51 51.84	18.288	46.644	0.080 ¹	A3111
03 16 09.82	-44 25 16.68	18.258	49.031	0.072 ³	A3112
03 17 54.00	-54 02 60.00	—	—	0.055 ³	S0339
03 20 10.54	-45 44 56.76	17.172	33.385	0.070 ¹	S0345
03 20 26.64	-24 59 19.32	18.848	32.755	0.086 ¹	
03 20 50.64	-53 20 22.20	17.989	48.744	0.078 ¹	
03 23 38.93	-58 45 35.99	17.766	36.963	0.067 ¹	
03 25 59.02	-53 53 06.72	17.017	39.791	0.059 ³	A3125
03 27 04.99	-53 11 38.04	17.238	39.836	0.060 ⁴	
03 27 23.50	-55 52 41.88	18.766	91.874	0.086 ³	A3126
03 27 51.12	-46 10 46.92	17.694	43.077	0.072 ¹	
03 29 07.94	-52 43 04.08	17.264	59.761	0.059 ³	A3128
03 33 03.46	-29 00 52.56	18.011	28.411	0.104 ¹	
03 34 04.82	-53 50 47.40	17.504	59.296	0.063 ¹	
03 34 46.56	-28 12 02.16	18.644	51.964	0.107 ¹	A3141
03 35 03.77	-39 57 15.48	18.795	55.795	0.103 ¹	A3142
03 36 24.79	-28 43 54.48	18.416	30.244	0.107 ¹	
03 36 28.68	-33 19 27.48	18.441	32.114	0.109 ¹	A3150
03 36 29.74	-25 10 48.36	18.259	28.941	0.053 ¹	
03 36 50.30	-40 45 08.28	18.400	25.432	0.062 ²	A3140
03 38 16.61	-28 50 32.28	17.985	43.401	0.068 ¹	A3151
03 39 05.30	-55 13 12.00	—	—	0.043 ³	A3144
03 39 26.88	-45 51 04.32	18.167	29.659	0.066 ¹	
03 41 42.29	-53 47 57.84	18.082	62.224	0.058 ³	A3158
03 43 21.12	-41 23 21.11	17.121	29.914	0.059 ¹	S0384
03 43 38.88	-24 25 58.44	19.110	48.669	0.105 ³	A0458
03 45 56.76	-17 48 21.60	17.916	49.562	0.149 ¹	A0462
03 46 11.57	-18 07 35.04	18.384	32.947	0.039 ¹	A3175
03 56 54.60	-30 21 37.80	18.720	46.929	0.098 ¹	A3194
03 57 47.30	-24 39 45.36	18.060	29.039	0.059 ¹	
04 06 07.75	-31 05 45.60	17.956	55.236	0.063 ¹	A3223
04 12 52.37	-55 07 40.08	18.621	32.986	0.099 ¹	

Table 4. (*continued*)

(1) $\alpha(1950)$	(2) $\delta(1950)$	(3) m_X	(4) \mathcal{R}	(5) z	(6) Abell
04 22 31.39	-27 52 12.72	17.006	29.468	0.048 ¹	S0449
04 24 07.46	-28 42 38.52	18.311	42.508	0.100 ¹	S0452
04 26 10.27	-28 21 11.52	17.260	28.386	0.094 ¹	S0459
04 27 51.55	-17 42 02.88	18.337	38.439	0.082 ¹	
04 30 02.90	-21 11 16.44	18.867	31.249	0.064 ¹	A3260
04 30 31.78	-61 31 51.96	18.120	47.493	0.059 ³	A3266
04 31 07.73	-32 46 03.01	17.648	29.637	0.116 ¹	A3269
04 33 32.83	-28 35 02.40	18.665	47.084	0.043 ¹	S0471
04 34 06.53	-22 32 39.12	17.305	36.703	0.069 ¹	S0473
04 36 36.29	-22 14 26.16	17.560	47.456	0.067 ³	A0500
04 38 25.37	-35 39 54.00	18.428	32.734	0.060 ¹	S0484
04 40 31.32	-32 52 42.96	17.719	35.885	0.080 ¹	S0491
04 44 39.60	-25 34 33.96	18.778	49.243	0.115 ¹	A0511
04 46 10.44	-20 33 14.40	17.819	45.751	0.073 ³	A0514
04 49 21.46	-51 12 24.85	18.819	34.581	0.093 ¹	S0502
04 59 03.99	-22 53 01.32	—	—	0.047 ³	A0533
04 59 12.67	-18 22 15.24	17.540	50.019	0.080 ¹	
05 08 14.66	-36 11 04.92	18.691	50.411	0.117 ¹	A3321
05 12 10.03	-41 47 58.93	18.771	53.283	0.081 ¹	
05 13 30.53	-49 07 20.28	18.751	68.344	0.091 ¹	A3330
05 14 38.47	-35 08 29.39	18.879	32.204	0.100 ¹	
05 15 01.75	-42 11 05.63	18.780	44.036	0.080 ¹	A3332
05 19 48.41	-40 54 25.21	18.755	28.825	0.077 ¹	A3336
05 23 51.94	-31 31 35.04	16.379	26.279	0.037 ¹	A3341
20 35 36.36	-61 24 36.36	16.742	43.854	0.071 ³	A3703
20 38 44.14	-35 25 40.81	18.300	62.379	0.090 ³	A3705
20 38 53.06	-61 35 31.20	17.231	33.611	0.093 ¹	
20 45 24.21	-62 11 03.12	17.855	30.340	0.108 ¹	
20 48 07.92	-52 56 04.92	15.741	44.932	0.047 ³	A3716
20 52 24.36	-36 10 35.39	18.881	28.133	0.087 ¹	
20 56 37.01	-35 36 11.52	18.379	26.185	0.092 ²	
20 57 40.80	-44 22 22.80	18.645	37.050	0.143 ¹	
21 02 53.91	-38 59 51.00	18.843	40.185	0.149 ¹	A3740
21 06 45.10	-27 16 16.68	17.959	28.561	0.103 ²	S0925
21 28 19.76	-43 30 26.64	18.695	32.332	0.105 ¹	A3775
21 29 13.29	-35 25 44.76	18.591	44.146	0.090 ¹	S0952
21 29 33.96	-24 11 38.40	18.446	29.428	0.063 ¹	
21 30 24.77	-31 28 53.40	17.479	32.326	0.065 ¹	
21 31 03.56	-53 51 02.52	17.591	32.325	0.078 ³	A3785
21 35 41.64	-51 41 01.32	18.235	27.928	0.094 ²	A3796
21 38 23.71	-34 13 37.20	18.132	28.347	0.077 ²	
21 39 10.27	-33 09 03.96	18.319	28.452	0.073 ²	
21 40 30.69	-39 14 34.80	17.919	40.173	0.066 ¹	S0964
21 42 13.73	-20 10 54.48	18.100	36.800	0.059 ¹	A2372
21 44 02.14	-44 07 21.36	18.068	29.345	0.062 ¹	A3809
21 45 22.44	-32 51 31.68	18.407	28.359	0.107 ²	A3812
21 49 31.83	-19 48 40.32	19.327	69.692	0.094 ³	A2384
21 55 52.56	-72 06 10.07	17.131	36.237	0.069 ²	
21 57 54.51	-43 24 12.60	18.610	33.570	0.070 ¹	
21 58 17.90	-60 11 05.63	18.470	40.567	0.099 ³	A3827
22 03 57.94	-46 00 13.68	18.585	37.280	0.076 ¹	
22 07 13.37	-65 46 11.27	18.027	32.926	0.075 ¹	
22 15 58.87	-24 28 39.72	16.674	28.325	0.039 ¹	

Table 4. (*continued*)

(1)	(2)	(3)	(4)	(5)	(6)
$\alpha(1950)$	$\delta(1950)$	m_X	\mathcal{R}	z	Abell
22 17 02.14	-55 28 18.84	—	—	0.040 ³	A3869
22 20 41.26	-55 28 48.00	18.301	32.149	0.078 ¹	
22 21 00.69	-61 52 34.68	18.543	42.807	0.122 ¹	
22 21 29.66	-64 30 37.44	18.967	39.439	0.094 ³	S1022
22 24 14.43	-69 16 24.24	17.435	28.356	0.068 ²	A3879
22 24 22.03	-49 09 19.08	18.668	53.851	0.097 ¹	A3877
22 27 23.95	-48 25 40.43	18.414	29.884	0.103 ¹	A3883
22 29 31.46	-25 41 55.68	16.542	26.256	0.035 ²	
22 30 05.18	-55 03 49.33	18.779	41.799	0.075 ³	A3886
22 33 36.05	-24 35 44.88	17.121	27.097	0.034 ¹	A3893
22 36 35.14	-17 36 24.48	17.844	39.867	0.074 ¹	A2462
22 39 49.18	-25 15 25.20	17.850	37.495	0.080 ²	
22 40 39.43	-59 28 51.95	18.807	34.216	0.083 ¹	
22 41 12.48	-45 47 34.80	18.490	30.986	0.093 ¹	
22 42 59.11	-46 10 34.32	18.851	33.839	0.091 ¹	A3910
22 43 29.21	-17 57 15.84	17.939	32.379	0.071 ¹	A2480
22 46 16.07	-64 39 17.28	18.315	53.466	0.096 ¹	A3921
22 46 44.91	-52 03 51.84	18.800	57.446	0.098 ¹	A3922
22 56 55.00	-68 53 03.48	18.867	39.081	0.087 ¹	S1078
22 57 20.76	-61 54 37.44	17.817	37.884	0.086 ¹	
22 59 33.70	-22 17 02.76	19.338	50.752	0.136 ³	A2521
23 02 54.94	-21 38 42.36	18.295	35.898	0.095 ³	A2528
23 05 55.22	-20 09 28.44	18.780	51.898	0.083 ³	A2538
23 09 08.51	-29 20 08.16	18.619	43.000	0.117 ¹	
23 09 36.52	-21 50 16.80	18.809	61.707	0.086 ³	A2556
23 14 36.24	-42 58 00.48	17.450	29.636	0.096 ¹	S1106
23 24 09.07	-24 07 30.00	18.467	43.173	0.088 ¹	A2599
23 25 31.71	-36 39 48.61	17.953	26.387	0.093 ²	
23 29 08.35	-34 24 50.03	17.043	28.615	0.051 ¹	A4012
23 33 32.54	-36 14 27.23	18.147	28.694	0.096 ¹	
23 34 15.02	-33 00 31.68	18.464	32.987	0.111 ¹	
23 36 58.94	-46 15 46.07	18.165	31.477	0.067 ¹	S1140
23 38 58.65	-29 28 03.00	17.605	27.438	0.063 ¹	
23 42 37.97	-26 14 49.56	17.037	33.693	0.052 ¹	A2660
23 53 05.28	-33 53 13.92	17.934	29.970	0.107 ¹	S1161
23 56 20.59	-60 55 55.20	19.318	47.358	0.096 ³	A4067
23 57 53.38	-66 47 34.44	18.096	27.320	0.073 ²	S1166
23 58 08.74	-49 50 03.48	17.900	27.576	0.067 ²	
23 59 44.06	-54 18 59.04	18.013	34.972	0.085 ²	

Notes to column (7) refer to the source of the redshift:

- 1 This work (AAT long-slit observation)
- 2 This work (A.N.U. 2.3m long-slit observation)
- 3 Data taken from Andernach (1989)
- 4 Obtained by cross-referencing with Huchra (1990)